2014

A New Dynamic Heat Exchanger Model with Frosting and Defrosting

Hongtao Qiao
University of Maryland, United States of America, htqiao@umd.edu

Vikrant Aute
University of Maryland, United States of America, vikrant@umd.edu

Reinhard Radermacher
University of Maryland, United States of America, raderm@umd.edu

A New Dynamic Heat Exchanger Model with Frosting and Defrosting

Hongtao QIAO[1]*, Vikrant AUTE[2], Reinhard RADERMACHER[3]

Center for Environmental Energy Engineering
Department of Mechanical Engineering, University of Maryland
College Park, MD 20742 USA
[1,2]Tel: 301-405-8726, [3]Tel: 301-405-5286, Fax: 301-405-2025
Email: [1]htqiao@umd.edu, [2]vikrant@umd.edu, [3]raderm@umd.edu

*Corresponding Author

ABSTRACT

In this paper, a dynamic heat exchanger model that unifies the frosting and defrosting analyses is presented. A novel scheme is proposed to solve the air flow redistribution due to non-uniform frost blockage. Unlike the existing defrost models which separate analysis for tubes and fins, the proposed defrost model unifies the analysis to maintain model consistency. The first-principles based frost and defrost models developed in this research allow for a more realistic assessment of the heat pump systems and greatly facilitate the design of controls. Utilizing the developed models, the transient behavior of a flash tank vapor injection heat pump under frosting and defrosting conditions is investigated and validated against experimental data.

1. INTRODUCTION

Air source heat pumps are used to transfer heat from outside to inside a building during winter. The outdoor coil works as an evaporator and frost might deposit on coil surfaces if the ambient temperature is lower than the freezing point. Frost accumulation on coil surfaces can appreciably degrade the performance of heat pumps by reducing the capacity of the system. This capacity degradation is caused by multiple phenomena such as: (1) Frost layer results in an additional thermal resistance; (2) Frost accumulation decreases the air flow rate; (3) Frost accumulation might lead to operating instability if a TXV is used in the system; (4) Defrosting cycle needs to be initiated periodically in order to remove frost buildup and free coil surfaces before the unit can return to deliver heating service again.

In order to design a system to minimize the adverse impacts of frost accumulation on the performance of the unit, numerous studies have been conducted to gain a better understanding about frost properties, frost growth process and the heat transfer characteristics.

Frost formation is a rather complex phenomenon involving simultaneous heat and mass transfer and it is difficult to analytically predict the frosting process. A common assumption adopted by the mathematical models is that the water vapor transported onto the frost surface from the air stream consists of two parts. A part of this water vapor directly diffuses into the frost layer to solidify the frost, while the remainder deposits on the frost surface to increase frost thickness (Sami and Duong; 1989). In general, fully transient models of frost accumulation are more attractive from modeling accuracy perspective since they usually account for the early stage of frost formation and the spatial variation of temperature and density within the frost layer (Tao *et al*., 1993; Le Gall *et al*., 1997; Chen *et al*., 2003). However, quasi-steady state models (Seker *et al*., 2004; Tso *et al*., 2006) are more favorable and more widely used in practice because 1) fully transient models are computationally expensive, and 2) the early stage of frost formation is thought to be of secondary interest while the period of frost growth is of primary interest.

It is well recognized that frost does not uniformly accumulate on the fan-driven coils because the coil surface temperature varies from the inlet to the outlet of the heat exchanger circuits and possible air flow maldistribution during the operation further aggravates this non-uniformity. Meanwhile, non-uniform frost deposition on coil surface will in turn affect the air flow distribution through the coil.

Air flow maldistribution has been shown to be one of the dominant factors that degrade the performance of the heat exchangers (Guo *et al*., 2008). Hence, it is wise to incorporate the effect of air flow redistribution when modeling

frost formation on the heat exchangers. However, a review of literature indicates that most of studies on frost formation on heat exchangers neglect this effect (Kondepudi and O'Neal, 1993; Seker *et al*., 2004; Tso *et al*., 2006; Yang *et al*., 2006; Silva *et al*., 2011) except a recent study by Padhmanabhan *et al*. (2011) who found that neglecting the air flow redistribution phenomenon imposes large errors in the simulation. However, a thorough review of the Padhmanabhan's work indicates that their model has the following limitations:

(1) First of all, the heat exchanger model is validated against experimental data obtained from an air-to-brine coil and there is no phase change on the brine side. This simplifies the study significantly because it is anticipated that phase transition on the tube side will exacerbate the non-uniformity of frost deposition onto the coil. Moreover, since it is a single-phase coil, the issue of refrigerant maldistribution does not show up to complicate the simulation.

(2) The air-to-brine coil has a very simple geometry (1 row coil with 12 one-pass horizontal tubes). In practice, the heat exchangers are often multi-row coils with complex asymmetric circuitries. The air flow propagation has significant influences on the frost distribution.

(3) As mentioned earlier, air flow maldistribution due to frost blockage can lead to hunting of a thermostatic valve. Therefore, the steady-state formulations for the refrigerant flow are not adequate and transient formulations are necessary if the heat exchanger model is integrated into a system simulation tool to investigate the transient characteristics of the entire system under frosting/defrosting conditions.

(4) Lastly, the significance of their work is to identify the effect of non-uniform frost accumulation on the air flow redistribution. Consequently, a large system of complex non-linear air pressure equalization equations needs to be solved simultaneously at each time step. This induces a great amount of computation burden to the entire solution process and hence slows down the simulation significantly. In Padhmanabhan's case, 48 air pressure equations in total need to be solved simultaneous at each time step (4 segments for each of total 12 tubes). In practice, however, heat exchangers are often much larger in size than this coil and more equations are required to be solved accordingly.

In light of these research gaps, a new first-principles based heat exchanger model is developed to address the above limitations. The proposed model is characterized with the following major features: (1) Unify the analysis for frosting and defrosting in a single model; (2) A segment-by-segment finite volume approach (can be simplified to a tube-by-tube approach); (3) Transient modeling on the refrigerant side to analyze unsteady flows; (4) A novel scheme is presented to solve the air flow redistribution by linearizing the system of non-linear air pressure drop equalization equations, which can significantly accelerate the simulation; (5) Unlike the existing defrost model (Dapozo *et al*., 2010) that separates the analysis for tubes and fins, the proposed model unifies the analysis to maintain model consistency.

This new heat exchanger model allows for a more realistic assessment of heat pump systems and greatly facilitates the design of controls. Utilizing the developed model, the transient behavior of a flash tank vapor injection heat pump system under frosting and defrosting conditions is investigated and validated using experimental data. For the sake of brevity, this paper will not present the details of the frost modeling and instead will focus on defrosting and air flow redistribution due to frost blockage.

2. MATHAMTICAL MODEL

2.1 Refrigerant Flow

For the sake of brevity, the modeling details on the refrigerant side are not presented here. Interested readers are referred to the paper by Qiao *et al*. (2014).

2.2 Frosting model

The frost sub-model are available in many papers (Seker *et al*., 2004; Tso *et al*., 2006; Yang *et al*., 2006) and hence is not repeated. This section only focuses on how to solve for the air flow redistribution due to non-uniform frost blockage. The air flow redistribution of the heat exchanger can be handled in a quasi-steady state fashion, i.e.

steady-state conditions is assumed to exist within sufficiently small time intervals, but the overall analysis will remain transient in nature.

As stated previously, to determine the time evolution of air flow distribution, a number of non-linear air pressure equalization equations need to be solved simultaneously at each time step. Considering the fact that the correlations for calculating air pressure drop are very complicated in general, the computation overhead associated with determining the air flow redistribution is substantial and results in a significant decrease in simulation speed. However, this process can be substantially simplified by taking advantage of the approximation that the state of the fan-coil system at the next time step can be regarded as a perturbed state near the equilibrium state at the current time step. In this way, the corrections to the air mass flow rate for each time step can be readily determined without solving the set of pressure equalization equations.

The analysis is started by assuming that one has already obtained the air flow rate across the i^{th} segment of j^{th} horizontal row at current time t, i.e. $\dot{m}_{i,j,t}$ and the total air volumetric flow rate delivered by the fan at the same time is $\dot{V}_{fan,t}$. The fan-coil system is assumed to operate steadily with this air flow distribution within the time interval between t and $t + \Delta t$ since Δt is sufficiently small. The air flow distribution remains unchanged until the arrival of the next time step, $t + \Delta t$. At the next time step $t + \Delta t$, both frost density and thickness increases due to frost accumulation, and the air flow distribution changes accordingly. Assume that the air flow rate across the i^{th} segment of the j^{th} horizontal row becomes $\dot{m}_{i,j,t+\Delta t} = \dot{m}_{i,j,t} + \Delta\dot{m}_{i,j}$ at $t + \Delta t$, and the total air volumetric flow rate that the fan delivers becomes $\dot{V}_{fan,t+\Delta t} = \dot{V}_{fan,t} + \Delta\dot{V}_{fan}$ at the same time. Obviously, the following expression holds

$$\Delta\dot{V}_{fan} = \frac{\sum_{i=1}^{M}\sum_{j=1}^{N}\Delta\dot{m}_{i,j}}{\rho_{fan,in,t+\Delta t}} \tag{1}$$

where $\rho_{fan,in,t+\Delta t}$ is the air density at the inlet to the fan.

Since Δt is quite small, the state of the fan-coil system at $t + \Delta t$ can be regarded as a perturbed state near the equilibrium state at time t. Hence, by utilizing the first order approximation, one can linearize the expression of air pressure drop as follows (note: the pressure drop terms are evaluated with the frost thickness at $t + \Delta t$, i.e. $\delta_f + \Delta\delta_f$)

$$\Delta p_{i,j,t+\Delta t} \approx \Delta p_{i,j,t} + \left.\frac{\partial\left(\Delta p_{i,j,t}\right)}{\partial\dot{m}_{i,j,t}}\right|_{\dot{m}_{i,j,t}} \Delta\dot{m}_{i,j} \tag{2}$$

$$\Delta p_{fan,t+\Delta t} \approx \Delta p_{fan,t} + \left.\frac{\partial\left(\Delta p_{fan,t}\right)}{\partial\dot{V}_{fan,t}}\right|_{\dot{V}_{fan,t}} \Delta\dot{V}_{fan} \tag{3}$$

where $i = 1, 2, \ldots, M$ (each tube is subdivided into M segments), $j = 1, 2, \ldots, N$ (the coil has N horizontal rows), and $x_{i,j}$ denotes a variable for the i^{th} segment on the j^{th} horizontal row. At time $t + \Delta t$, the fan-coil system operates at another equilibrium state and is subject to the following constraints

$$\begin{aligned} \Delta p_{1,1,t+\Delta t} &= \Delta p_{fan,t+\Delta t} \\ \Delta p_{1,2,t+\Delta t} &= \Delta p_{fan,t+\Delta t} \\ &\cdots \\ \Delta p_{M,N,t+\Delta t} &= \Delta p_{fan,t+\Delta t} \end{aligned} \tag{4}$$

$$\text{Let } A=\sum_{i=1}^{M}\sum_{j=1}^{N}\frac{1}{\left.\frac{\partial\left(\Delta p_{i,j,t}\right)}{\partial \dot{m}_{i,j,t}}\right|_{\dot{m}_{i,j,t}}},\quad B=\sum_{i=1}^{M}\sum_{j=1}^{N}\frac{\Delta p_{i,j,t}}{\left.\frac{\partial\left(\Delta p_{i,j,,t}\right)}{\partial \dot{m}_{i,j,t}}\right|_{\dot{m}_{i,j,t}}}$$

$$\Delta\dot{V}_{fan}=\frac{\frac{B}{A}-\Delta p_{fan,t}}{\left.\frac{\partial\left(\Delta p_{fan,,t}\right)}{\partial \dot{V}_{fan,t}}\right|_{\dot{V}_{fan,t}}-\frac{\rho_{fan,in,t+\Delta t}}{A}} \tag{5}$$

All the terms in Equation (5) can be computed explicitly. In general, the partial derivatives of air pressure drop with respect to the air mass flow can be evaluated analytically if the correlation is given. Therefore, Equation (5) provides a mean to readily determine the time evolution of air volumetric flow rate of the fan. Figure 1 compares the proposed approach of calculating the air flow redistribution with Padhmanabhan's approach. It can be noted that the proposed approach can directly solve the air flow distribution for each time step without iteration. Elimination of iteration significantly speeds up the simulation (more than 10 times faster), especially for large coils.

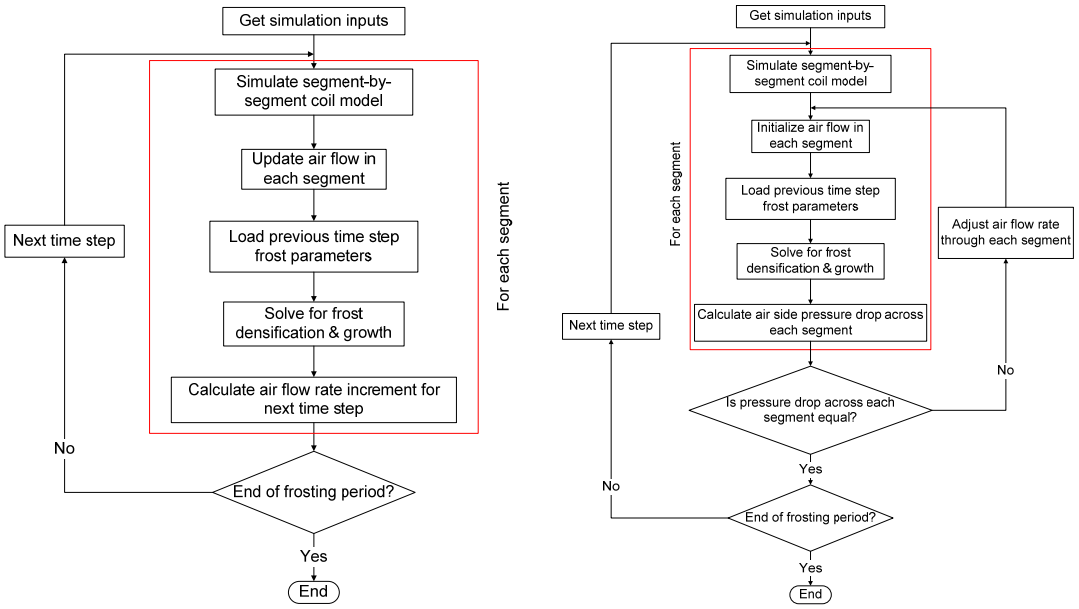

Figure 1: Comparison between the proposed approach (left) and Padhmanabhan's approach (right)

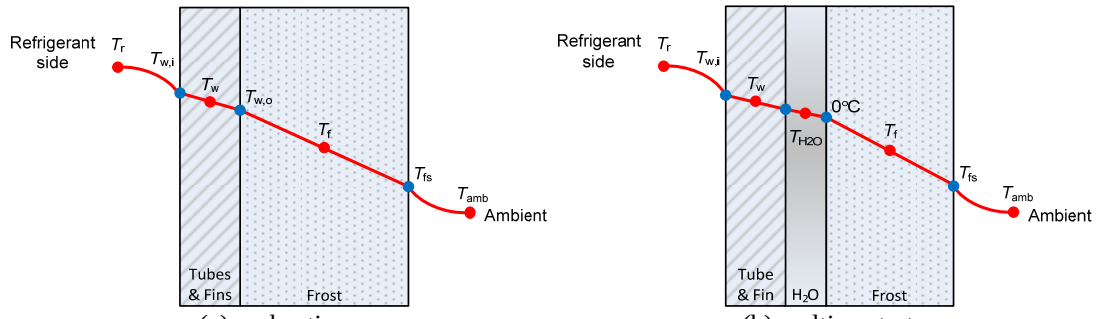

(a) preheating (b) melting start

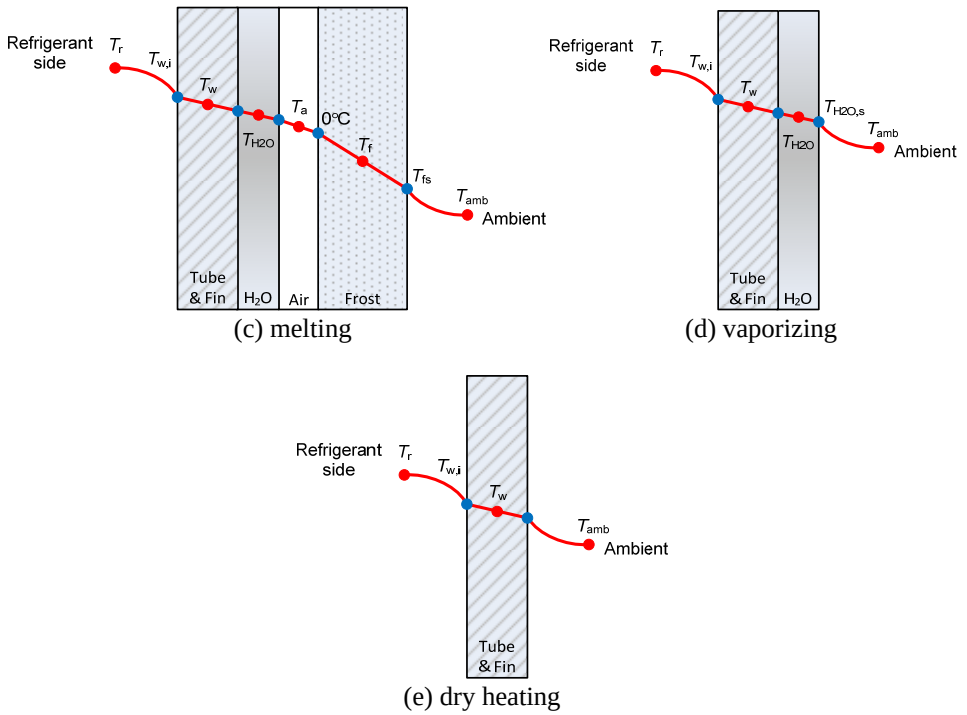

Figure 2: Temperature profile for the five-stage defrosting model

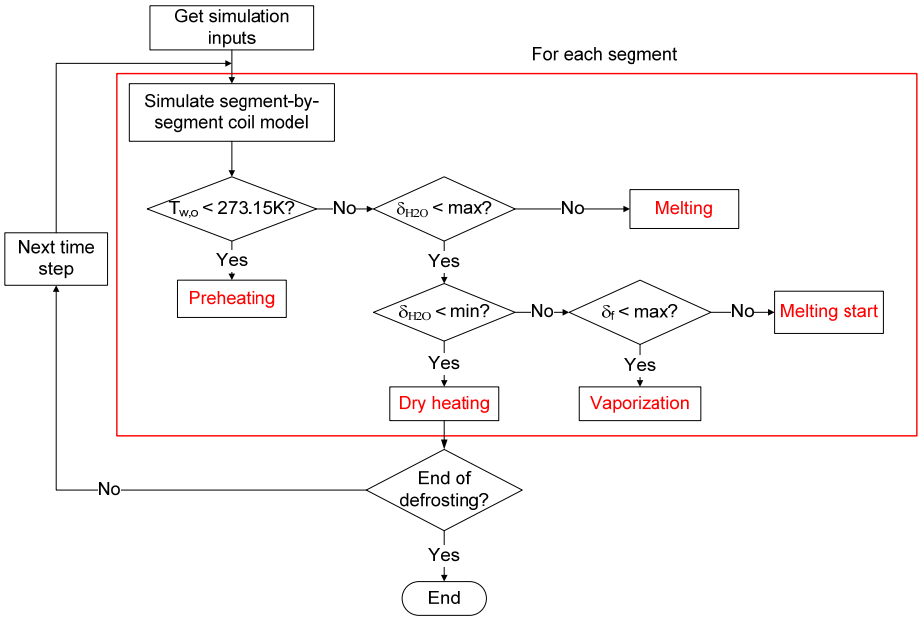

Figure 3: Algorithm for defrosting model

2.3 Defrosting model

The reverse-cycle defrosting process is divided into five stages: preheating, melting start, melting, vaporizing and dry-heating. Figure 2 shows the temperature profile for each stage. Figure 3 shows the algorithm of the model.

Preheating stage: This stage comes to an end when the temperature at the interface between the tube/fin surfaces and frost reaches to 273.15K. During this stage, there is no phase change, and only the temperatures of the system increase. Equation (6) - (11) are the governing equations for this stage.

$$\alpha_i\left(T_r - T_{w,i}\right) = k_w \frac{T_{w,i} - T_w}{\delta_w / 2} \tag{6}$$

$$\rho_w c_{p,w} \delta_w \frac{dT_w}{dt} = k_w \frac{T_{w,i} + T_{w,o} - 2T_w}{\delta_w / 2} \tag{7}$$

$$k_w \frac{T_w - T_{w,o}}{\delta_w / 2} = k_f \frac{T_{w,o} - T_f}{\delta_f / 2} \tag{8}$$

$$\rho_f c_{p,f} \delta_f \frac{dT_f}{dt} = k_f \frac{T_{w,o} + T_{fs} - 2T_f}{\delta_f / 2} \tag{9}$$

$$k_w \frac{T_{w,o} - T_w}{\delta_w / 2} = k_f \frac{T_f - T_{w,o}}{\delta_f / 2} \tag{10}$$

$$\begin{aligned} k_f A_o \frac{T_f - T_{fs}}{\delta_f / 2} = \dot{m}_a c_{p,a}\left(T_{fs} - T_a\right)\left[1 - \exp\left(-\frac{\alpha_o A_{o,eff}}{\dot{m}_a c_{p,a}}\right)\right] \\ + \Delta h_{ig} \dot{m}_a \left(\omega_a - \omega_{fs}\right)\left[1 - \exp\left(\frac{\alpha_o A_{o,eff}}{\dot{m}_a c_{p,a} Le^{2/3}}\right)\right] \end{aligned} \tag{11}$$

Melting start stage: After the preheating stage, the frost starts to melt and a water film appears between the tube/fin and frost. As the frost continues to melt, the thickness of the water film increases until it reaches its maximum thickness. Equation(6), (7), (12) - (16) are the governing equations for this stage.

$$k_w \frac{T_w - T_{w,o}}{\delta_w / 2} = k_f \frac{T_{w,o} - T_{H_2O}}{\delta_{H_2O} / 2} \tag{12}$$

$$\rho_{H_2O} c_{p,H_2O} \delta_{H_2O} \frac{dT_{H_2O}}{dt} = k_{H_2O} \frac{T_{w,o} + 273.15 - 2T_{H_2O}}{\delta_{H_2O} / 2} \tag{13}$$

$$-\Delta h_{if} \rho_f \frac{d\delta_f}{dt} = k_{H_2O} \frac{T_{H_2O} - 273.15}{\delta_{H_2O} / 2} + k_f \frac{T_f - 273.15}{\delta_f / 2} \tag{14}$$

$$\rho_f c_{p,f} \delta_f \frac{dT_f}{dt} = k_f \frac{273.15 + T_{fs} - 2T_f}{\delta_f / 2} \tag{15}$$

$$\delta_{H_2O} = \delta_f\big|_{t=0} - \delta_f \tag{16}$$

Melting stage: After the water film reaches its maximum thickness, the melted frost will drain off. A gap appears between water and the frost. The volume formerly occupied by the water is replaced by surrounding air. During this stage, the thickness of the water film is fixed at its maximum thickness. This stage ends when the frost is completely melted. Equation (6), (7), (12), (17) - (20) are the governing equations for this stage.

$$\rho_{H_2O} c_{p,H_2O} \delta_{H_2O} \frac{dT_{H_2O}}{dt} = k_{H_2O} \frac{T_{w,o} - T_{H_2O}}{\delta_{H_2O} / 2} + \frac{T_a - T_{H_2O}}{\frac{\delta_a}{2k_a} + \frac{\delta_{H_2O}}{2k_{H_2O}}} \tag{17}$$

$$-\Delta h_{if}\rho_f \frac{d\delta_f}{dt} = k_a \frac{T_a - 273.15}{\delta_a / 2} + k_f \frac{T_f - 273.15}{\delta_f / 2} \tag{18}$$

$$\rho_a c_{p,a}\delta_a \frac{dT_f}{dt} = \frac{273.15 - T_a}{\frac{\delta_a}{2k_a}} + \frac{T_{H_2O} - T_a}{\frac{\delta_{H_2O}}{2k_{H_2O}} + \frac{\delta_a}{2k_a}} \tag{19}$$

$$\delta_a = \delta_f\big|_{t=0} - \delta_{H_2O,\max} - \delta_f \tag{20}$$

Vaporizing stage: This stage ends when the retained water completely vaporizes. Equation (6), (7), (12), (21) - (23) are the governing equations.

$$\rho_{H_2O} c_{p,H_2O}\delta_{H_2O} \frac{dT_{H_2O}}{dt} = k_{H_2O} \frac{T_{w,o} - T_{H_2O}}{\delta_{H_2O} / 2} + k_{H_2O} \frac{T_{H_2O} - T_{H_2O,s}}{\delta_{H_2O} / 2} \tag{21}$$

$$\rho_{H_2O} \frac{d\delta_{H_2O}}{dt} = c_{sv}\left(\rho_{H_2O,amb} - \rho_{H_2O,s}\right) \tag{22}$$

$$k_{H_2O} \frac{T_{H_2O} - T_{H_2O,s}}{\delta_{H_2O} / 2} = \alpha_o\left(T_{H_2O,s} - T_{amb}\right) + c_{sv}\left(\rho_{H_2O,s} - \rho_{H_2O,amb}\right)\Delta h_{fg} \tag{23}$$

Dry heating stage: The stage starts when there is no water retention on the surfaces, i.e. the water thickness is less than its minimum value. Once this stage is reached, it means that the defrosting process is completed. Equation (6), (7) and (24) are the governing equations.

$$k_w A_o \frac{T_w - T_{w,o}}{\delta_w / 2} = \dot{m}_a c_{p,a}\left(T_{w,o} - T_a\right)\left[1 - \exp\left(-\frac{\alpha_o A_{o,eff}}{\dot{m}_a c_{p,a}}\right)\right] \tag{24}$$

3. CASE STUDY AND SIMULATION RESULTS

Utilizing the developed models, the transient behavior of a flash tank vapor injection (FTVI) heat pump system under frosting and defrosting conditions is investigated. The studied system and its log(p)-h diagram are shown in Figure 4. The high pressure and high temperature vapor (2) discharged by the compressor enters the condenser. The refrigerant passing through the condenser rejects heat to the high temperature reservoir and changes to a subcooled liquid (3). Then, the refrigerant flows through the upper-stage expansion valve undergoing a drastic drop in pressure and temperature. This process results in a vapor-liquid mixture entering the flash tank (4) where vapor and liquid separates. The saturated vapor (6) is injected to the compressor. The saturated liquid (5) flows through the lower-stage expansion valve undergoing another throttling process. The low pressure, low temperature and low quality refrigerant (7) enters the evaporator, where it picks up heat from the low temperature reservoir, reaching a superheated vapor state (1) at the evaporator exit. The compressor receives refrigerant at state 1 and compresses it to an intermediate pressure during the first compression stage (8) after which the refrigerant mixes with injected vapor. Finally, the mixed refrigerant (9) is further compressed to a high pressure during the second compression stage. The compression process is associated with an increase in refrigerant temperature.

The detailed modeling techniques for other components are presented in Qiao *et al.* (2012 & 2014). The operating condition was that the indoor temperature was at 21°C (48% RH) and the outdoor temperature was at 1.7°C (82% RH).

Figure 5 compares the simulation results with experimental data for the FTVI system under the frosting cycle. Figure 5a) shows the transients of the pressures. It can be seen that the suction pressure declines as time goes by because of the decreasing air flow rate resulting from frost blockage. Accordingly, the intermediate pressure and

discharge pressure decline as well. After 3000 seconds, the pressures start to oscillate due to two underlying reasons: (1) the lower-stage TXV starts to hunt due to the decreased suction pressure; and (2) the upper-stage EEV synchronizes with TXV in order to control the injection superheat at this time because the liquid level in the flash tank varies periodically. TXV hunting can be verified by observing the transients of suction superheat shown in Figure 5b). Figure 5c) shows the variations of heat loads.

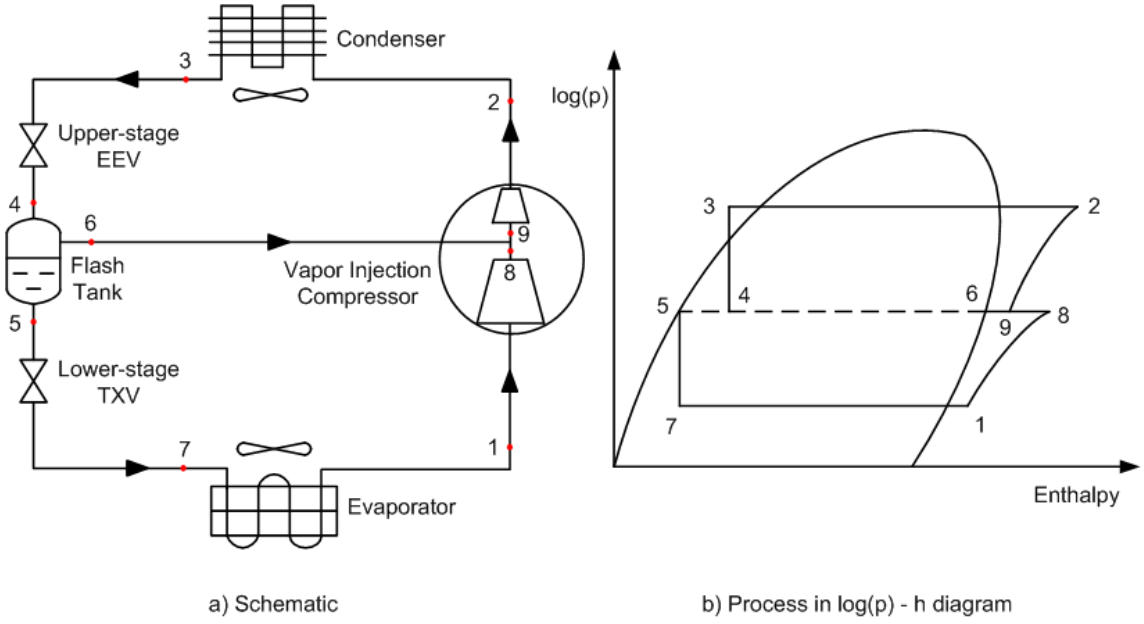

Figure 4: FTVI system

The discrepancies between the simulation results and experimental data lie in two aspects. One aspect is that the experiment is conducted with enabling the control of upper-stage EEV. Due to the hysteresis effect of the EEV, it is extremely difficult to predict the refrigerant mass flow through the valve. Since the EEV opening changes drastically at the beginning of start-up, the simulated pressure transients do not agree very well with the experiment. The other aspect lies in that outdoor coil air flow rate used in the simulation might deviate from the actual air flow rate during the experiment because of lack of measurements.

For the defrosting cycle, unfortunately, there are no good experimental data to validate our model. Hence, we only conduct a case study to demonstrate the model capabilities. Figure 6a) shows the pressure transients of the FTVI system undergoing the transition between the frosting cycle and defrosting cycle. Before 3000 seconds, the system runs in the heating mode. After 3000 seconds, the system initiates the defrosting cycle. During the defrosting period, the system is reversed and the upper-stage EEV is fully open and the outdoor coil fan is still on. The system is reversed at 3000 seconds. Soon after the system is reversed, the pressures equalize. Finally, the pressures stabilize at much lower values. The entire defrosting process lasts for about 600 seconds. Figure 6b) shows the variations of frost thickness on each tube during the defrosting cycle.

4. CONCLUSIONS

A dynamic heat exchanger model that unifies the frosting and defrosting analyses is presented. A novel scheme is proposed to solve the air flow redistribution by linearizing the system of non-linear air pressure drop equalization equations, which can significantly accelerate the simulation. Utilizing the developed models, the transient behavior of a flash tank vapor injection heat pump under frosting and defrosting conditions is investigated. Comparison between the simulation results and experimental data indicates that the proposed model can reasonably predict the pressure and temperature trends. Future work includes the validation for the defrosting model.

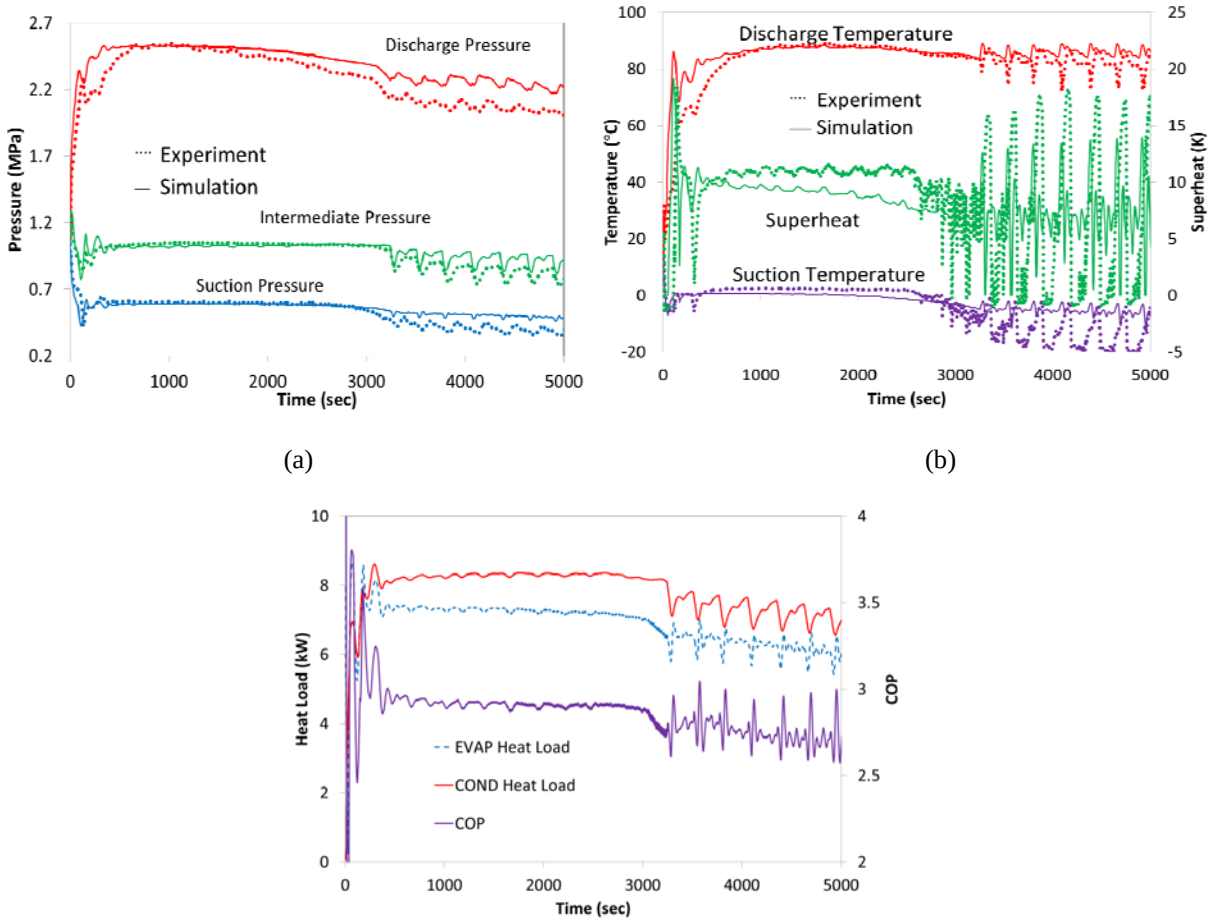

Figure 5: Results for the frosting period - (a) pressure transients; (b) transients of temperatures and suction superheat; (c) transients of heat loads and COP

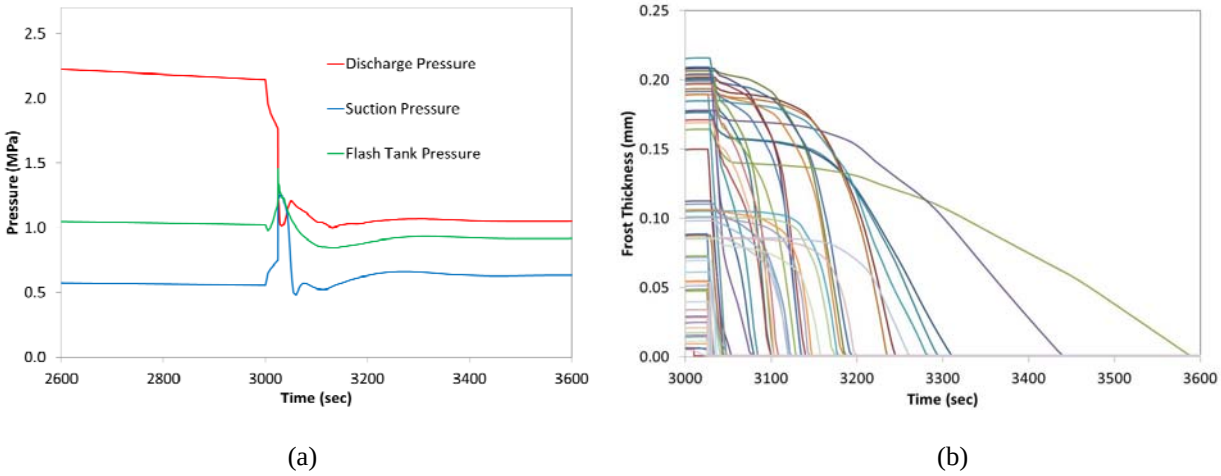

Figure 6: (a) Simulated pressure transients; (b) Simulated frost thickness on each tube

NOMENCLATURE

A	area [m^2]	*Subscripts*	
c_p	specific heat [J/kg-K]	amb	ambient
c_{sv}	mass transfer coefficient [kg/m^2-s]	eff	effective
h	enthalpy [J/kg]	f	frost
k	thermal conductivity [W/m-K]	fan	fan
Le	Lewis number [-]	fg	liquid to vapor surface
M	number of horizontal rows [-]	fs	frost surface
$\dot{m}$	mass flow rate [kg/s]	H_2O	water
N	number of segments [-]	i	internal
p	pressure [Pa]	if	ice to liquid
T	temperature [K]	ig	ice to vapor
t	time [s]	in	inlet
δ	thickness [m]	max	maximum
ω	humidity ratio [kg dry air/kg H_2O]	o	external
ρ	density [kg/m^3]	r	refrigerant
α	heat transfer coefficient [W/m^2-K]	s	surface
Δ	difference [-]	w	tube wall

REFERENCES

Chen, H., Thomas, L., Besant, R.W., 2003. Fan supplied heat exchanger fin performance under frosting conditions. *Int. J. Refrigeration* 26, 140-149.

Dopazo, J.A., Fernandez-Seara, J., Uhía, F.J., Diz, R., 2010. Modeling and experimental validation of the hot-gas defrost process of an air-cooled evaporator. *Int. J. Refrigeration* 33, 829-839.

Guo, X.M., Chen, Y.G., Wang, W.H., Chen, C.Z., 2008. Experimental study on frost growth and dynamic performance of air source heat pump system. *Applied Thermal Engineering* 28(17-18), 2267-2278.

Kondepudi, S.N. and O'Neal, D.L., 1993. Performance of finned-tube heat exchangers under frosting conditions: I. Simulation model. *Int. J. Refrigeration* 16(3), 175-180.

Le Gall, R., Grillot, J.M., Jallut, C., 1997. Modeling of frost growth and densification. *Int. J. Heat Mass Transfer* 40(13), 3177-3187.

Padhmanabhan, S.K., Fisher, D.E., Cremaschi, L., Moallem, E., 2011. Modeling non-uniform frost growth on a fin-and-tube heat exchanger. *Int. J. Refrigeration* 34, 2018-2030.

Qiao, H., Aute, V., Radermacher, R., 2014. Transient modeling of a flash tank vapor injection heat pump system. Part I - model deveopment. *Int. J. Refrigeration*. (Under review)

Qiao, H., Xu, X., Aute, V., Radermacher, R., 2012. Modelica-based transient modeling of a flash tank vapor injection system. 14th *International Refrigeration and Air Conditioning Conference at Purdue*, West Lafayette, IN, USA, Paper No. 2186.

Sami, S.M. and Duong, T., 1989. Mass and heat transfer during frost growth. *ASHRAE Transactions* 95(1), 158-165.

Seker, D., Karatas, H., Egrican, N., 2004. Frost Formation on Fin-and-Tube Heat Exchangers. Part I - Modeling of Frost Formation on Fin-and-Tube Heat Exchangers. *Int. J. Refrigeration* 27, 367-374.

Silva, D.L. Da, Hermes, C.J.L., Melo, C., 2011. First-principles Modeling of Frost Accumulation on Fan-supplied Tube-Fin Evaporators. *Applied Thermal Engineering* 31(14-15), 2616-2621.

Tao, Y.X., Besant, R.W., Rezkallah, K.S., 1993. A mathematical model for predicting the densification and growth of frost on a flat plate. *Int. J. Heat Mass Transfer* 36(2), 353-363.

Tso, C.P., Cheng, Y.C., & Lai, A.C.K., 2006. An improved model for predicting performance of finned tube heat exchanger under frosting condition, with frost thickness variation along fin. *Applied Thermal Engineering*, 26(1), 111-120.

Yang, D.K., Lee, K.S., Song, S., 2006. Modeling of prediction frosting behavior of a fin-tube heat exchanger. *Int. J. Heat Mass Transfer* 49, 1472-1479.